A model of cochlear mechanics with outer hair cell motility

Stephen T. Neely
Boys Town National Research Hospital, 555 North 30th Street, Omaha, Nebraska 68131

(Received 18 December 1991; accepted for publication 22 March 1993)

The outer hair cell (OHC) is known to have the ability to change its length in response to voltage changes across its membrane. The apparent function of this OHC motility is to enhance the tuning of the basilar membrane. The model presented in this paper represents the displacement-to-voltage and voltage-to-displacement transducers of the OHC explicitly, each as low-pass filter functions. The model results show that this OHC representation is sufficient to provide a model of cochlear mechanics with mechanical tuning at the inner hair cell which is comparable to the threshold tuning curves observed in single auditory nerve fibers. The enhancement of tuning provided by OHC motility can be interpreted as the combined action of a *cochlear amplifier* and a *second filter*. This model demonstrates that realistic cochlear tuning does not require intrinsic resonance in any cochlear structure other than the basilar membrane.

PACS numbers: 43.64.Kc, 43.64.Bt, 43.64.Ld

INTRODUCTION

The cochlea is the principal hearing organ of the mammalian auditory system. Sensory cells within the cochlea are arranged in rows which extend from one end of the cochlea to the other and are capable of detecting incredibly small (less than 1 nm) vibrations. These sensory cells are called "hair cells" because of tiny (1-μm diameter) projections at one end, through which the cell is able to detect motion. There are two groups of hair cells: the *inner* hair cells (IHC) and *outer* hair cells (OHC). The role of the IHCs is to send messages to the brain about the presence of acoustic vibrations at a specific place in the cochlea. The role of the OHCs is to influence these mechanical vibrations before they reach the IHCs.

Outer hair cells are cylindrically shaped and are known to be able to change their length in response to changes in the voltage across their cell membrane (e.g., Brownell *et al.*, 1985; Santos-Sacchi, 1989). In this paper, a model of cochlear mechanics is presented in which the motility of OHCs has a strong influence on the sharpness of both basilar membrane and IHC tuning. The present model is a refinement of earlier models of Neely and Kim (1983,1986) and incorporates recent information about OHC motility.

I. MODEL EQUATIONS

The cochlea is a long, narrow, fluid-filled tunnel which spirals through the temporal bone. This tunnel is divided along its length by a cochlear partition (CP) into an upper compartment called *scala vestibuli* (SV) and a lower compartment called *scala tympani* (ST). At the *base* of the cochlea is the middle-ear, where acoustic vibrations are transmitted into SV through the footplate of the stapes. A flexible boundary called the round window is at the basal end of ST. At the *apex* of the cochlea, SV and ST are connected to each other by the *helicotrema*.

The equations used to model the mechanics of the cochlea are described below in the frequency domain with assumed $e^{i\omega t}$ time dependence. A single spatial dimension x is used to represent the length of the cochlea (along its spiral course) with $x=0$ at the stapes and $x=L$ at the helicotrema. The term *macromechanics* is used to refer to the mechanics of the fluid in SV and ST and the interaction of the fluid with its boundaries at the stapes, round window, helicotrema, and CP. The term *micromechanics* refers to the movement and interaction of the structures within the CP.

A. Macromechanics

To simplify the macromechanics, we divide the cochlea into a large number of thin slices cut perpendicular to the x axis. Since the cochlea is spiraled, these slices are referred to as *radial cross sections* (RCS). Each RCS has a thickness δ, which may vary as a function of place. It is assumed (again for simplicity) that the RCSs are mechanically coupled to adjacent sections only through the fluid compartments (SV and ST); any longitudinal coupling directly through the CP is ignored (Viergever, 1978). The fluid mechanics are typically reduced to one dimension assuming a long-wave approximation (e.g., Viergever and Diependaal, 1986). The model equation for fluid pressure is derived here in order to include dependence on cross-sectional area and viscous damping of longitudinal fluid motion in a simple manner.

Figure 1 summarizes the representation of the macromechanics in this model for a single RCS at a distance x from the stapes. The combined mass of the SV and ST is lumped into a single mass element $M_f(x)$. The value assigned to this acoustic mass element is computed as

$$M_f(x)=2\rho\delta/A_c(x), \tag{1}$$

where ρ is the fluid density and $A_c(x)$ is the "average" cross-sectional area of SV and ST. The value of the damping parameter $R_f(x)$ is chosen as required for proper cochlear input impedance at low frequencies. The total acoustic admittance for the fluid in a single RCS is

$$Y_f(x)=[R_f(x)+i\omega M_f(x)]^{-1} \tag{2}$$

 0001-4966/93/94(1)/137/10/$6.00

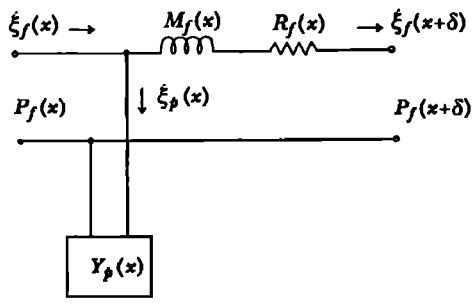

FIG. 1. Summary of cochlear macromechanics for one radial cross section. The volume velocity entering this section is $\dot{\xi}_f(x)$ and the fluid pressure at this point is $P_f(x)$. The volume velocity of the cochlear partition in this section is $\dot{\xi}_p(x)$ which is opposed by the acoustic admittance $Y_p(x)$. The mass and damping of the scala fluid are represented by $M_f(x)$ and $R_f(x)$. (Electrical symbols are used to represent the mechanical elements in this and other figures in order to show connections between the individual mechanical components more clearly.)

and defines the relation between fluid pressure and volume velocity

$$\dot{\xi}_f(x+\delta)=Y_f(x)[P_f(x)-P_f(x+\delta)]. \tag{3}$$

The difference between the volume velocity $\dot{\xi}_f(x)$ entering this RCS and the volume velocity $\dot{\xi}_f(x+\delta)$ leaving this RCS is the volume velocity $\dot{\xi}_p(x)$ of the CP:

$$\dot{\xi}_p(x)=\dot{\xi}_f(x)-\dot{\xi}_f(x+\delta). \tag{4}$$

The volume velocity of the CP can also be computed as

$$\dot{\xi}_p(x)=Y_p(x)P_f(x), \tag{5}$$

where $Y_p(x)$ is the acoustic admittance of the CP (described in detail below) and $P_f(x)$ is the fluid pressure difference across the CP.

Therefore, the RCS at x is coupled to the two adjacent RCSs by the following equation

$$[Y_p(x)+Y_f(x-\delta)+Y_f(x)]P_f(x)$$
$$=Y_f(x-\delta)P_f(x-\delta)+Y_f(x)P_f(x+\delta), \tag{6}$$

for $0<x<L$. Equation (5) (together with appropriate boundary conditions) represents the macromechanics of the cochlear model. The RCS at the apical boundary $x=L$ is terminated by a damping element R_h representing fluid passage through the helicotrema:

$$[R_h+Y_f(x-\delta)]P_f(x)=Y_f(x-\delta)P_f(x-\delta). \tag{7}$$

The RCS at the basal boundary $x=0$ is attached to the middle-ear which is described in the next section.

B. Middle ear

In order to facilitate comparison of model results with experimental measurements, a simple representation of the middle-ear is included as summarized in Fig. 2. The input to the middle-ear is specified in terms of sound pressure P_e at the eardrum. The mechanical admittance of the middle-ear is defined as

$$Y_m=[K_m/(i\omega)+R_m+i\omega M_m]^{-1}. \tag{8}$$

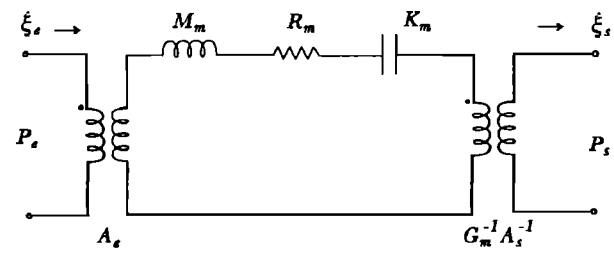

FIG. 2. Summary of middle-ear mechanics. The input to the middle ear is specified by the pressure at the eardrum P_e. The output of the middle ear is represented by the volume velocity of the stapes footplate is $\dot{\xi}_s$ and the fluid pressure at stapes P_s. The mass, damping, and stiffness of the middle-ear ossicles are represented by the mechanical elements M_m, R_m, and K_m. The lever gain of the middle ear is g_m, the effective area of the eardrum is A_e, and the area of the stapes footplate is A_s.

The middle-ear is coupled to the cochlea by assuming that the pressure at the stapes is $P_s=P_f(0)$ and that the volume velocity at the stapes is $\dot{\xi}_s=\dot{\xi}_f(0)$. If we also require that the CP has zero admittance at $x=0$, then

$$\dot{\xi}_f(0)=g_mA_sA_eY_mP_e-(g_mA_s)^2Y_mP_f(0), \tag{9}$$

where g_m is the "lever gain" of the middle-ear ossicles, A_e is the effective area of the eardrum, and A_s is the area of the stapes footplate. This middle-ear model is a simplified version of the model described by Matthews (1980). Matthews included flexibility in the connection between malleus and stapes which is not included here and which will influence the model above 10 kHz.

C. Micromechanics

The anatomical structure of a radial cross-section (RCS) of the cochlear partition (CP) is illustrated in Fig. 3. In the present model, the basilar membrane (BM) and

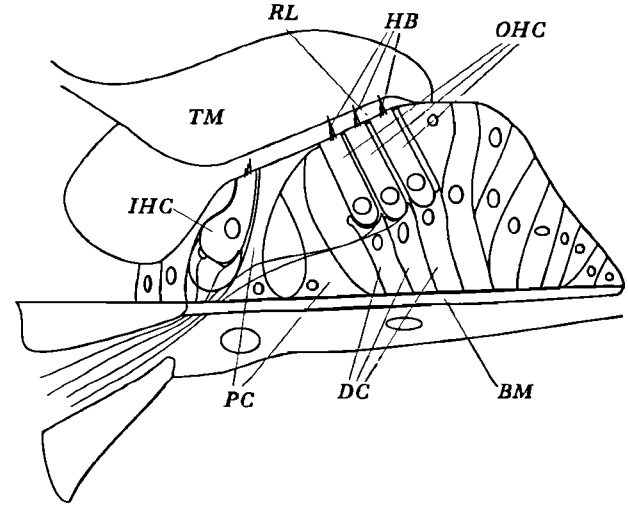

FIG. 3. Anatomical structure of the cochlear partition. The outer hair cells (OHC) and inner hair cells (IHC) are positioned between the basilar membrane (BM) and reticular lamina (RL). The tips of the hair bundles (HB) of the OHC are embedded in the tectorial membrane (TM). The base of the OHC is resting on the cup of the Deiter cell (DC). The IHC and OHCs are separated by rigid pillar cells (PC). The HB of the IHC do not touch the TM and are displaced by viscous fluid drag.

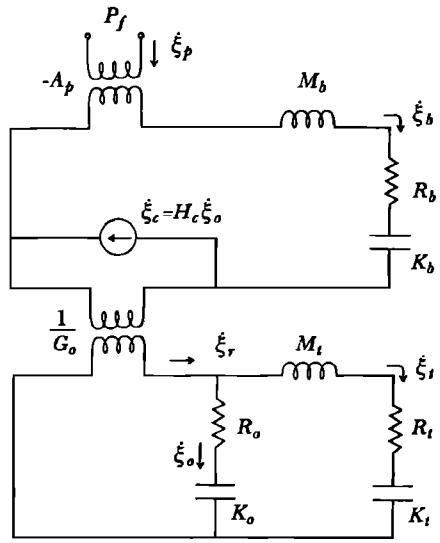

FIG. 4. Summary of cochlear micromechanics for one radial cross section. The input to the cochlear partition consists of the fluid pressure P_f and volume velocity of the partition $\dot{\xi}_p$. The effective area of the partition in this section is A_p. (The minus sign on A_p is because $\dot{\xi}_p$ and $\dot{\xi}_b$ are defined as positive in opposite directions.) The upper loop in this figure includes the mass, damping, and stiffness of the basilar membrane (BM) M_b, R_b, and K_b. Contraction of the outer hair cell (OHC) is represented by a velocity source $\dot{\xi}_c=H_c\dot{\xi}_o$. The lower loop includes the mass, damping, and stiffness of the tectorial membrane (TM) M_t, R_t, K_t. The BM and TM are coupled through the lever gain g_o. The stiffness of the OHC hair bundles and the viscous damping of the subtectorial fluid are represented by K_o and R_o.

the tectorial membrane (TM) are each represented as a lumped mass with both stiffness and damping in their attachment to the surrounding bone. It is assumed in this model that the effect of outer hair cell (OHC) contraction is to change the separation between the BM and the reticular lamina (RL) in a manner similar to the models suggested by Geisler (1986), by Jones and Kim (1988), and by Geisler and Shan (1991). The amount of contraction ξ_c is assumed to be directly related to lateral deflection ξ_o of the hair bundle (HB) at the top of the OHC by an OHC gain function H_c that is described below:

$$\xi_c=H_c\xi_o. \tag{10}$$

(The x dependence is not shown explicitly in this section in order to simplify the equations.)

Figure 4 shows a summary of the micromechanics for a single RCS. The effective area of the CP for this section is

$$A_p=b_w\delta, \tag{11}$$

where b is the effective width of the BM. The velocity $\dot{\xi}_b$ of the BM is assumed to be directly proportional to the volume velocity $\dot{\xi}_p$ of the CP

$$\dot{\xi}_p=-A_p\dot{\xi}_b. \tag{12}$$

The minus sign appears in Eq. (11) because ξ_p is defined as positive for displacement toward ST and ξ_b is defined as positive for displacement toward SV. The mechanical admittances of the BM and TM are

$$Y_b=[K_b/(i\omega)+R_b+i\omega M_b]^{-1}, \tag{13}$$

$$Y_t=[K_t/(i\omega)+R_t+i\omega M_t]^{-1}. \tag{14}$$

The mechanical impedance which couples the BM and TM is

$$Z_o=K_o/(i\omega)+R_o. \tag{15}$$

The displacement ξ_o of the HB is the difference between lateral displacement ξ_r of the RL and lateral displacement ξ_t of the TM,

$$\xi_o=\xi_r-\xi_t. \tag{16}$$

The lateral RL displacement ξ_r is assumed to be proportional to BM displacement ξ_b minus any contraction ξ_c of the OHC

$$\xi_r=g_o(\xi_b-\xi_c). \tag{17}$$

From these equations we can derive the acoustic admittance of the CP

$$Y_p=A_p^2Y_b(1+g_oH_oZ_oY_b)^{-1}, \tag{18}$$

where H_o is the transfer function that relates ξ_o to ξ_b

$$H_o=\xi_o/\xi_b=g_o(1+g_oH_c+Z_oY_t)^{-1} \tag{19}$$

and H_c is the OHC gain function and will be described in the next section.

D. Outer hair cell

The motility of OHCs is represented in the model by an OHC gain function which describes the ratio of OHC contraction to HB deflection. The OHC gain function is the product of two separate transducer functions: (1) mechanoelectric transduction (forward transduction) at the HB and (2) electromechanic transduction (reverse transduction) at the lateral membrane of the OHC. In this model a first-order, *low-pass* filter function is used to represent each of the two transducers

$$T_f=g_f/(1+i\omega\tau_f), \tag{20}$$

$$T_r=g_r/(1+i\omega\tau_r). \tag{21}$$

The forward transduction T_f describes the ratio of receptor potential to HB displacement. The reverse transduction T_r describes the ratio of OHC length contraction to receptor potential.

The mechanoelectric transduction T_f at the midpoint of the CP is similar to what has been observed by Denk and Webb (1989) as a result of Brownian motion in a hair cell from a frog sacculus. The electromechanic transduction T_r is similar to that observed by Santos-Sacchi (1991) in an outer hair cell from a guinea pig.

The place dependence of these transducer functions was determined primarily by what was needed in the cochlear model to simulate neural tuning curves. The complete OHC gain function is the product of the mechanoelectric and electromechanic transduction:

$$H_c=\gamma T_fT_r, \tag{22}$$

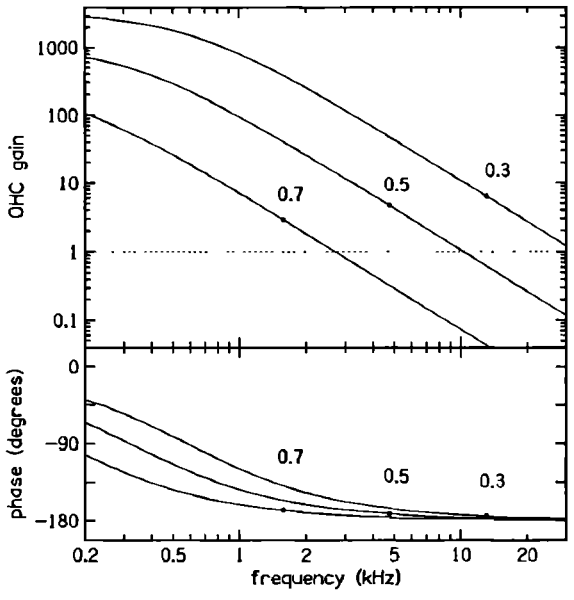

FIG. 5. OHC gain function. The OHC gain is defined as the product of the forward and reverse transduction shown in the previous two figures. The curves in this figure describe the decrease in cell length relative to hair bundle deflection at three places in the model, $x/L=0.3,0.5,0.7$. The circles on each curve indicate the characteristic frequency for corresponding place.

where γ is simply a multiplier (normally set equal to 1) used to demonstrate the effects of impaired OHC motility. The OHC gain function used in the model calculation is shown in Fig. 5.

E. Inner hair cell

To simulate neural tuning, we must also calculate the displacement of the HB of the IHC. It is assumed that the HB is not in contact with the TM and is displaced by fluid drag. Consequently, the HB displacement is proportional to fluid displacement at high frequencies and proportional to fluid velocity at low frequencies. The transition frequency will be denoted by f_c.

It is also assumed that the shearing displacement between TM and RL in the vicinity of the inner hair cells is *less* affected (by a fraction α) by OHC contraction than is the HB deflection of the OHC. This could be due to the presence of the rigid pillar cells between IHCs and OHCs. Therefore, the displacement ξ_i of the HB of the IHC is computed as

$$\xi_i=\{g_o[\xi_o-(1-\alpha)\xi_c]-\xi_t\}[1+2\pi f_c/(i\omega)]^{-1}. \quad (23)$$

The transfer function that relates ξ_i to ξ_b becomes

$$H_i=\xi_i/\xi_b=H_o(1+\alpha g_o H_c)[1+2\pi f_c/(i\omega)]^{-1}. \quad (24)$$

The observed effect of α being nonzero is that it causes the "tails" of the tuning curves to differ between IHCs and OHCs.

II. MODEL RESULTS

Model parameters were chosen primarily so that the IHC hair bundle displacement ξ_i exhibited tuning similar to that observed in single auditory nerve fibers in cat. It was also required that the model results show reasonable agreement with cochlear input impedance, BM displacement, and OHC receptor potential.

TABLE I. Model parameter values as a function of x. Parameter values were specified at $x=0$, $x=L/2$, and $x=L$. Values at other locations were interpolated by fitting a quadratic polynomial to the log of the parameter values at the specified locations. See the text for the values of other parameters.

Parameter	$x=0$	$x=L/2$	$x=L$	Units
A_c	5.52×10^{-3}	3.17×10^{-3}	4.27×10^{-3}	cm^2
α	0.081	0.035	0	
K_b/A_p	1.14×10^{8}	4.19×10^{6}	5.97×10^{4}	dyn cm^{-3}
K_t/A_p	1.99×10^{4}	2.21×10^{4}	3.16×10^{4}	dyn cm^{-3}
K_o/A_p	1.05×10^{4}	9.23×10^{3}	1.25×10^{4}	dyn cm^{-3}
M_b/A_p	9.14×10^{-6}	9.60×10^{-6}	1.06×10^{-5}	g cm^{-2}
M_t/A_p	5.64×10^{-4}	1.02×10^{-3}	1.06×10^{-2}	g cm^{-2}
R_b/A_p	2.08×10^{-2}	2.03×10^{-2}	1.88×10^{-2}	dyn cm^{-3} s
R_t/A_p	149	63.4	27.0	dyn cm^{-3} s
R_o/A_p	2037	282	38.0	dyn cm^{-3} s
g_f	1.42×10^{5}	1.05×10^{4}	3.68×10^{2}	nm^{-1} mV
g_r	0.1	0.1	0.1	nm mV^{-1}
τ_f	1.40×10^{-4}	6.92×10^{-4}	5.29×10^{-3}	s
τ_r	1.35×10^{-4}	3.61×10^{-4}	2.50×10^{-3}	s

The values of the chosen model parameters which vary with x are listed in Table I. Other parameter values which do not vary with x are: $\gamma=1$, $\rho=1$, $L=2.5$ cm, $f_c=1.39$ kHz, $K_m=1.5\times10^5$ dyn cm^{-1}, $R_m=15$ dyn cm^{-1} s, $M_m=5\times10^{-3}$ g, $A_s=1\times10^{-2}$ cm^2, $A_m=15\times10^{-2}$ cm^2, $g_m=0.5$, $R_f=2\cdot10^5$ dyn cm^{-5} s, $b_w=0.01$ cm, $\delta=0.005$ cm, $g_o=1$, and $R_h=6.94\cdot10^4$ dyn cm^{-5} s. The model results presented below are based on numerical solution of the frequency-domain model equations described above using these parameter values.

A. Input to the cochlea

The acoustic input impedance Z_c to the cochlea was computed from the model results according to the formula

$$Z_c=\frac{P_f(0)}{Y_f(0)[P_f(0)-P_f(\delta)]}. \quad (25)$$

The model input impedance is shown in Fig. 6 and compared with a model of Lynch *et al.* (1981) which is based on their experimental measurements in a cat. The ratio of pressure at the stapes P_s to pressure at the eardrum P_e in the model is shown in Fig. 7 and compared with the experimental measurements of Nedzelnitsky (1980) in a cat. Although there is general agreement between the model and the data, the reader should note the substantial difference at 4 kHz of about 20 dB in magnitude and 90 deg in phase.

B. Neural tuning curves

The most important result presented in this paper is that a cochlear model with plausible OHC transducer characteristics is able to simulate the tuning of neural threshold tuning curves, as shown in Fig. 8. The dashed lines represent the averaged neural response threshold

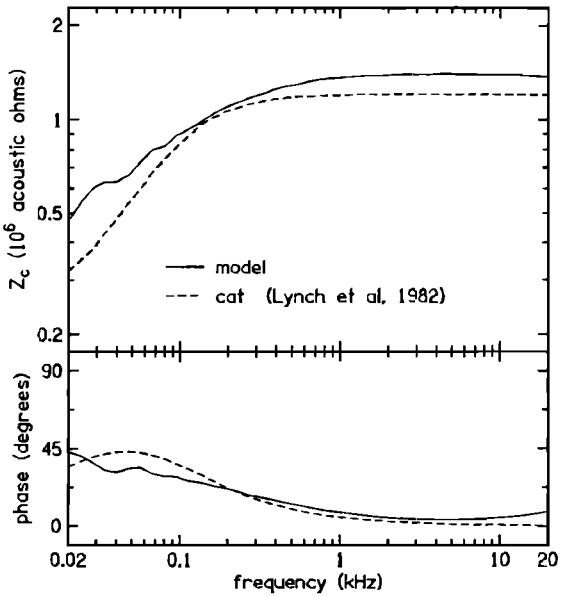

FIG. 6. Cochlear input impedance. The acoustic input impedance of the cochlea is defined as the ratio of pressure at the stapes to volume velocity of the stapes footplate. The solid line is derived from the cochlear model using Eq. (24) in this paper. The dashed line is from a simple model derived by Lynch *et al.* (1981) to fit their measurements of stapes pressure and velocity in a cat.

from six chamber-raised cats (Liberman, 1978). The solid lines in Fig. 8 shows *isodisplacement* curves from the model using the criterion ξ_i=0.3 nm. The tuning curves in this figure span the seven octaves from 0.25 to 32 kHz and show good agreement between the model and the measured data.

In addition to the magnitude of the neural response, it is important to also consider its phase and latency. The model IHC tuning is compared in Fig. 9 with three neural

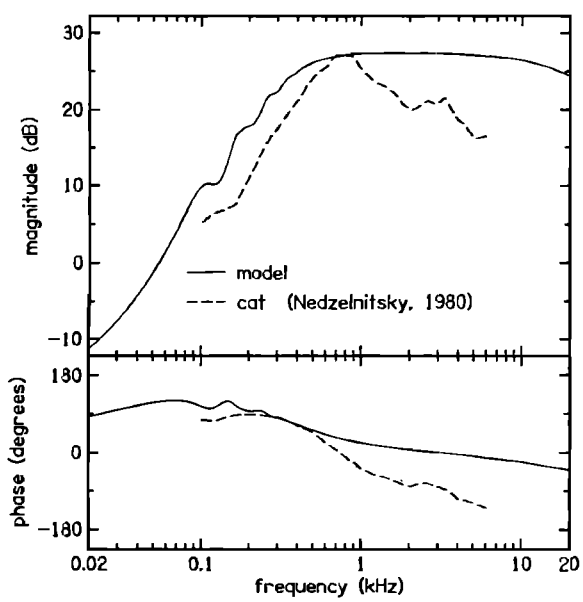

FIG. 7. Middle-ear transfer function. The model result (solid line) for the ratio of the fluid pressure at the stapes P_s to the sound pressure at the eardrum P_e is compared with the pressure ratio observed by Nedzelnitsky (1980) in a cat.

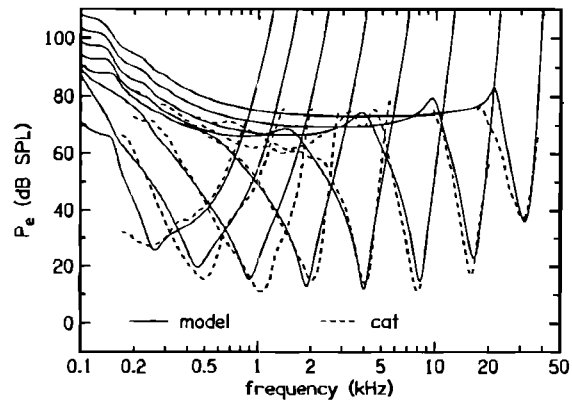

FIG. 8. IHC tuning curves. Isodisplacement curves (solid lines) from the model using the criterion ξ_i=0.3 nm are compared with neural threshold tuning curves (dashed lines) obtained by Liberman (1978) from single nerve fibers of cats. The ordinate indicates the sound pressure (P_e) required at the eardrum to elicit the criterion response.

response tuning curves from a cat for which group delay (defined as minus the slope of the phase with respect to frequency) was also measured (Allen, 1983). In Fig. 10, the model results for ξ_i are compared with the magnitude and phase responses of a population of cat nerve fibers (Kim *et al.*, 1979) at two different stimulus frequencies, 620 and 1550 Hz. In both Figs. 9 and 10 the model shows

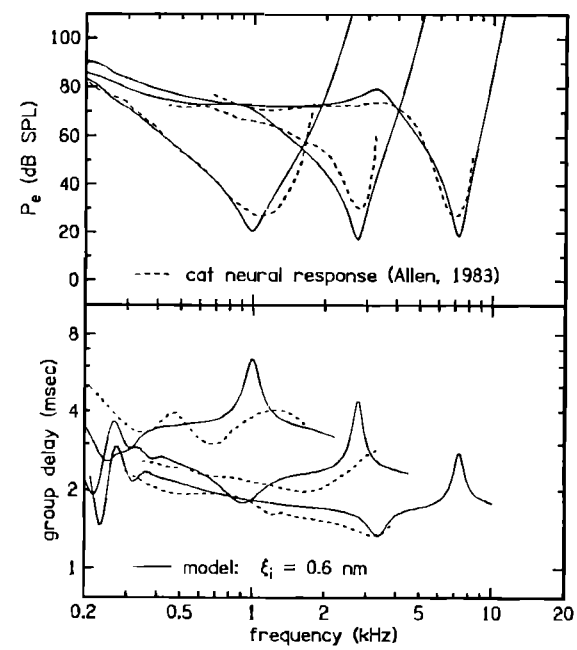

FIG. 9. IHC tuning curves with group delay. The neural response threshold tuning curves (dashed lines) in the upper panel are similar to those in Fig. 8. The model isodisplacement curves (solid lines), however, are for ξ_i=0.6 nm, indicating a 6 dB difference in either the sensitivity of the nerve fibers or threshold criterion used in their measurement compared with the neural data in the previous figure. The group delay in the lower panel is defined as minus the slope of the phase with respect to frequency. The neural group delay was measured at levels above the threshold level indicated in the upper panel and may change as a function of level. A constant delay of 1.2 ms was added to the model group delay to compensate for the acoustic propagation and synaptic delay present in the measured data.

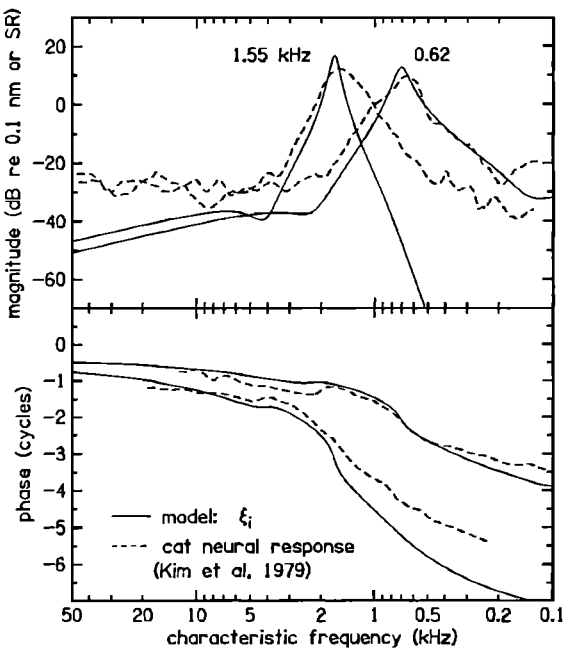

FIG. 10. IHC response curves at two frequencies as a function of CF. The solid lines represent ξ_i for the model with a stimulus level of 20 dB SPL; the magnitude is in dB *re*:0.1 nm. The dashed lines represent the Fourier component of period histograms obtained from many single nerve fibers in a cat (Kim *et al.*, 1979); the magnitude is in dB *re*:spontaneous rate (SR) of the fiber. Part of the reason for the difference between the magnitude of ξ_t and the neural data is the limited dynamic range of the nerve fiber between threshold and saturation. A constant phase of 1.2 ms times the frequency was added to each of the model phase curves to compensate for the acoustic propagation and synaptic delay present in the measured data.

reasonable agreement with the measured data with respect to phase and latency.

C. Displacements within the cochlear partition

To illustrate the differences in tuning among the various micromechanical structures of the cochlear partition, Fig. 11 shows the frequency response of three displacement variables ξ_b, ξ_o, ξ_i at three places x/L=0.3,0.5,0.7. This figure illustrates the degree of similarity between the IHC and BM tuning. The sharpness of tuning is very similar at the characteristic frequency (CF), but the tip-to-tail ratio is much larger for the IHC.

Figure 12 illustrates the point that the sharp tuning in this model is due to the OHC motility and not due to any resonance in the TM. In other words, this model does not incorporate a resonant TM and represents an alternative to resonant TM models (e.g., Allen, 1980). The magnitude and phase of ratio of ξ_r to ξ_b is shown by the solid lines in Fig. 12. These curves describe the additional tuning provided by the OHC to the RL in the model over what is present at the BM. The ratio of ξ_t to ξ_r is shown by the dashed lines in Fig. 12. These curves illustrate the negligible contribution of the TM to the tuning of the IHC.

Figure 13 shows the amount of OHC contraction relative to BM displacement at three places. The circles on each curve indicate the CF for the corresponding place. Note that the maximum magnitude of OHC contraction is

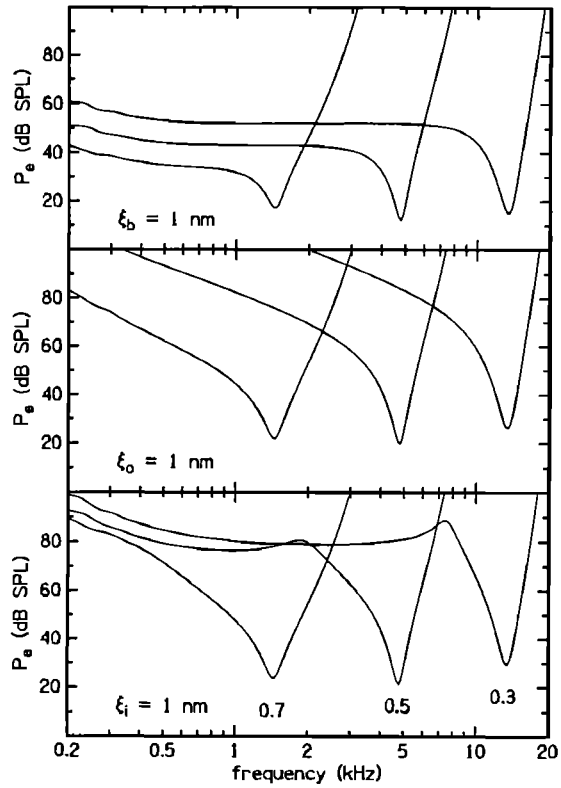

FIG. 11. Comparison of BM, OHC, and IHC tuning. The curves represent 1-nm isodisplacement of ξ_b, ξ_o, and ξ_i at three places x/L=0.3, 0.5, 0.7. The BM, OHC, and IHC tuning curves are similar in sharpness at their tips and differ primarily in their low-frequency tails.

(at most) about twice the BM displacement. The phase of OHC contraction at the CF is approximately −90 deg relative to BM displacement. Forces exerted on the BM at this phase can be interpreted as *negative damping* forces because they are 180 deg out of phase with BM damping forces.

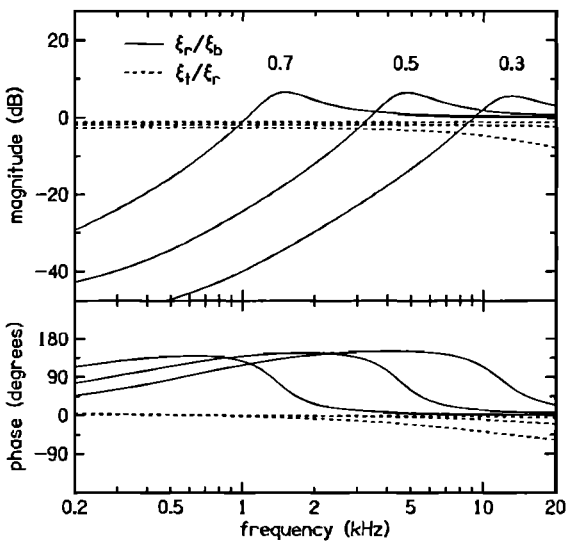

FIG. 12. Comparison of the tuning of RL and TM. The solid lines represent the ratio of ξ_r to ξ_b and the dashed lines represent the ratio of ξ_t to ξ_r at three places x/L=0.3, 0.5, 0.7. This comparison emphasizes the lack of any TM resonance in the present model.

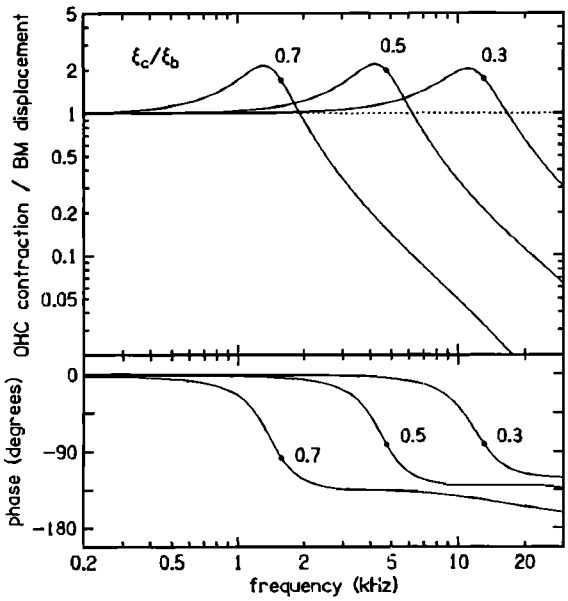

FIG. 13. OHC contraction relative to BM displacement. The curves represent the ratio of ξ_c to ξ_b at three places x/L=0.3, 0.5, 0.7. The circles indicate the characteristic frequency (CF) of the corresponding place. This figure shows that OHC contraction is maximum at a frequency slightly below CF and that the phase of OHC contraction at CF is about −90 deg, which is the "negative damping" phase.

D. Loss of OHC gain

The most physiologically vulnerable part of the cochlear micromechanics is thought to be the mechanoelectric transduction at the HB. OHC damage can be simulated in the model by reducing the value of the OHC gain parameter γ. Figure 14 shows the effect on IHC tuning ξ_i of setting γ to zero. The loss of the "tip" of the tuning curve and downward shift in the "tail" is similar to the effect on neural threshold tuning curves observed by Liberman and Dodds (1984) in cats with damaged OHCs.

Figure 15 shows the effect of loss of OHC gain on BM tuning. The upper panel shows *isodisplacement* curves for 1 nm BM displacement based on the Mössbauer measurements of Sellick *et al.* (1982). The three curves in the upper panel show the loss of sharp tuning as the condition of the animal deteriorated. The lower two panels show model results for the same isodisplacement criterion for ξ_b and ξ_c with γ=1, γ=0.7, and γ=0.5. The decrease in CF, decrease in high-frequency slope, and decrease in sensitivity of the model results when the parameter γ was decreased are all similar to what is observed in the experimental data.

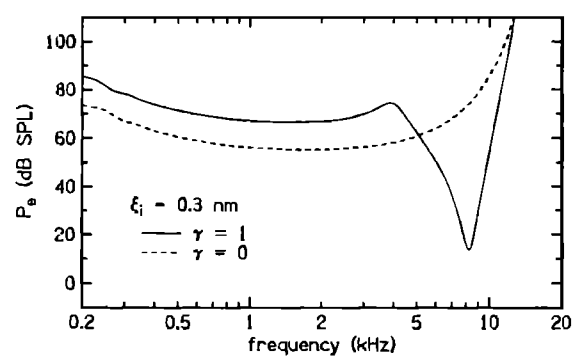

FIG. 14. Effect of loss of OHC gain on IHC tuning. The solid line represents the normal isodisplacement of ξ_i=0.3 nm at the 8 kHz place with γ=1. The dashed line shows the change in tuning when OHC contraction is completely eliminated by setting γ=0. The change in shape of the tuning curve is similar to that observed by Liberman and Dodds (1984) due to severe OHC damage.

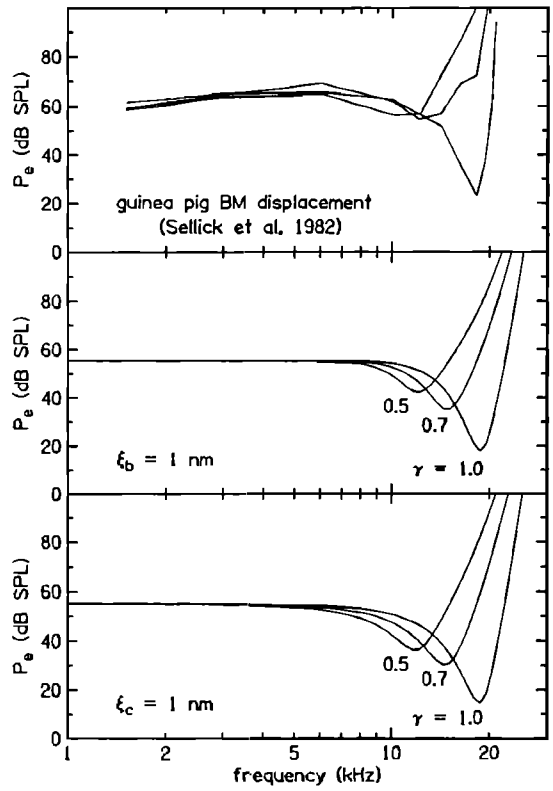

FIG. 15. Effect of loss of OHC gain on BM tuning. The upper panel shows 1 nm BM isodisplacement based on Mössbauer measurements in a guinea pig (Sellick *et al.*, 1982). The middle and lower panels show model results for ξ_b and ξ_c with γ=1, 0.7, 0.5. The measured change in tuning with deterioration in the condition of the cochlea is similar to the change in tuning observed in the model with reduction of the parameter γ.

Figure 16 shows the effect on the "second filter" (the ratio of ξ_i to ξ_b) of setting the mechanoelectric transducer gain g_f to zero. This second filter improves the tip-to-tail ratio of IHC tuning by 20 to 30 dB, but the improvement goes away with loss of OHC motility.

E. OHC receptor potential

One of the advantages of having an explicit representation of the OHC transducers in the model is that the OHC receptor potential can also be computed. Figure 17 shows the computed OHC receptor potential for the model at 0 dB SPL. For comparison, Dallos (1986) measured a receptor potential in a guinea pig of about 4 μV at 0 dB SPL in an OHC with a best frequency of 800 Hz. Similar measurements of Cody and Russell (1987) indicate a receptor potential of about 2 μV in a guinea pig OHC with a best frequency of 17 kHz. The model results do not conflict with these data.

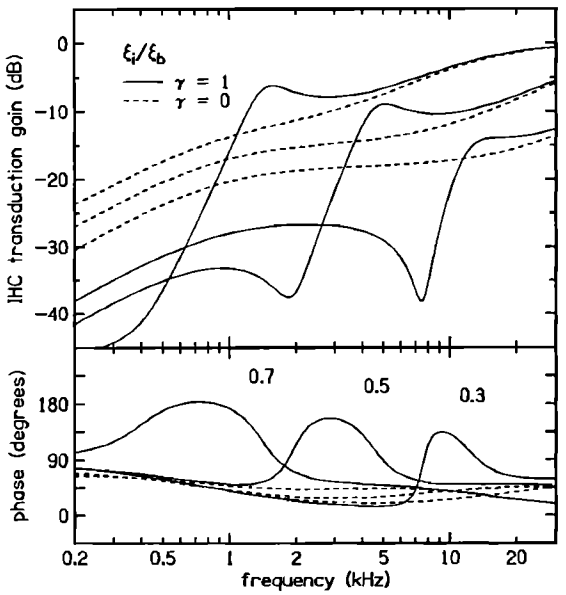

FIG. 16. Effect of loss of OHC gain on the "second filter." The solid lines represent the ratio of ξ_i to ξ_b at three places for the normal case when $\gamma=1$. The dashed lines show the loss of additional tuning provided by this "second filter" when $\gamma=0$.

III. DISCUSSION

The main purpose of this modeling effort is to provide a framework for understanding cochlear mechanics. The present model does not provide a completely realistic explanation for how the cochlea works. Some of the strengths and weaknesses of the model are discussed in this section.

A. Strengths

The cochlear model presented in this paper goes further than any previous model in relating plausible OHC transducer characteristics to neural threshold tuning. The principal differences between the model described in this paper and the model of Neely and Kim (1986) are (1) that OHC motility is represented as a change in the displacement between the BM and the RL instead of as a pressure source and (2) there is no intrinsic resonance in the TM. The OHCs in this model have a great influence on cochlear tuning because of the gain they provide to the mechanical feedback loop within the micromechanics of the cochlea. The OHCs are not required to have any intrinsic resonance and would exhibit only a "low-pass" frequency response when observed in isolation. The explicit representation of the OHC receptor potential in this model provides an independent check on the appropriateness of the assumed OHC characteristics.

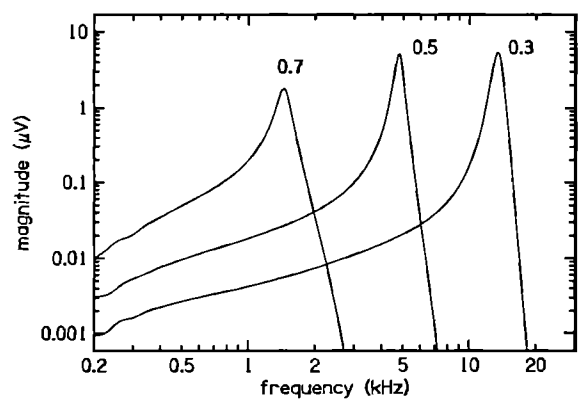

FIG. 17. OHC receptor potential at 0 dB SPL. The curves show the model results for OHC voltage at three places as a function of frequency.

The most significant feature of the OHC gain function is that the OHC contraction is greater than the HB deflection for frequencies below CF (i.e., the gain is greater than 1). The contraction of the OHC influences the deflection of its own HB. The relative phase of this feedback determines whether the OHC length change attenuates or amplifies the acoustic signal delivered to the IHC.

The assumed electromechanic transducer characteristics are generally consistent with the *in vitro* observations of OHC motility of Ashmore (1987), Santos-Sacchi (1989), and Evans *et al.* (1991). However, the observation of narrow, bandpass tuning by Brundin *et al.* (1989) is not supported by the present model. There is no doubt that the model is an oversimplification of the OHC and a more complete model of the OHC may exhibit bandpass tuning; however, the present model demonstrates that bandpass tuning need not be present in isolated OHCs. Further investigation is needed to determine whether OHCs really do possess bandpass tuning *in vivo*. We need to know more about OHC characteristics and how they change from base to apex.

The cochlear model described in this paper builds on the works of others. It places active elements near the sensory detectors, as suggested by Gold (1948). It provides a negative feedback loop which influences BM motion, as suggested by Mountain *et al.* (1988). It sets up a region of "negative damping" which acts as a traveling-wave amplifier, as suggested by Kim *et al.* (1980). And it includes a second-filter with a prominent "spectral zero" as suggested by Allen. The present model is unique in combining these ideas in a single model and in representing "active elements" explicitly in terms of OHC transducer functions.

Model parameters tend to be more sensitive to small changes in active models than in passive models because the most sensitive model conditions are often on the verge of instability. The present model has the advantage of less sensitivity to small changes in model parameters when compared to previous models described by Neely and Kim (1983, 1986). For example, there is no need for a close balance between positive and negative parameters as required by the model of Neely and Kim (1983) and the loss of tuning curve sensitivity with reduction of the parameter γ is much smaller than in the model of Neely and Kim (1986).

B. Weaknesses

Some of the basic modeling assumptions have had significant effects on the model results presented in this paper. The long-wave approximation commonly used in most models of cochlear mechanics; however, it is probably inadequate in the vicinity of the maximum response where the wavelength on the basilar membrane becomes shorter

than the height of the scalae. The effect of the long-wave assumption has not been investigated in the present model.

Because there are local sources within the cochlea in this model, the stability of model solutions in the time domain becomes an important question. The fact that the input impedance to the cochlea (shown in Fig. 6) has a positive real part for all frequencies suggests stability of the model. The fact that the slope of the basilar membrane response with respect to place was observed to be negative near the base for all frequencies investigated also suggests stability of the model. An example of the negative phase slope is shown indirectly by the responses at two frequencies in Fig. 10. The time-domain stability of the present model has not yet been established.

Model parameters were adjusted by a curve fitting program to improve the agreement between the model solutions and the neural data. Consequently, some of the model parameters may be unrealistic. For example, the mass of the basilar membrane seems to be unreasonably small. The need for such a small mass in this model may be related to the inadequacy of the long-wave approximation. The forward transduction gain parameter is larger at low frequencies than can be justified from experimental data; however, the resulting receptor potential shown in Fig. 17 is not inconsistent with experimental measurements.

The effect of the cochlear amplifier on the driving-point impedance of the cochlear partition is to (1) reduce the imaginary part (making it less negative) near the characteristic place, (2) make the real part negative on the basal side of the characteristic place (CP), and (3) make the real part more positive on the apical side of the CP. One consequence of the negative-damping region (where the real part of the impedance is negative) is that the cochlear traveling wave experiences a power gain. For example, at 8 kHz the present model provides a 28 dB power gain when the total power absorbed by the cochlear partition is compared with the total power entering the cochlea through the stapes. This power gain may be unrealistic since it requires as much as 28 attowatts (10^{-18} W) from a single OHC at 20 dB SPL. An alternative modeling strategy proposed by Kolston *et al.* (1990) places emphasis on reducing the imaginary part of the driving-point impedance to achieve improved sensitivity with much less (or no) power required from the OHC. Such an approach may be necessary in order to reduce the power requirement placed on the OHC by the present model.

Any pure delay (latency) associated with OHC transduction will have a significant influence on the phase of the OHC gain function, but has not been represented explicitly in this model. Geisler (1991) has included OHC transduction latency in a model of cochlear mechanics and shown how it influences mechanical responses. The OHC gain function in the present model should, perhaps, be modified to include a pure delay. The additional phase lag due to this delay will require that one or both of the time constants τ_f and τ_r be reduced to maintain the same combined phase at CF.

The distinction between ξ_o and ξ_i in the present model was made, primarily, to simulate the "tail" of the neural threshold tuning curve. The low-frequency response was attenuated too much by the OHC contraction. The definition of ξ_i was made in order to obtain a response which was not attenuated as much at low frequencies. One interpretation of the parameter α being nonzero is that the RL bends slightly at its attachment to the rigid pillar cells. Another possibility is that the OHC gain function in the present model is too large at low frequencies.

Many features of the cochlear model are, in various ways, oversimplified and might be represented in more detail in a more complete model. There is always a trade-off in models between complexity and completeness. In particular, the fluid mechanics and OHC transducer functions are probably inadequately represented. However, the present model does appear to demonstrate the basic function of the OHC, BM, and TM in an appropriate way and, consequently, provides considerable insight into how these elements function together in the cochlea. Furthermore, the OHC gain function shown in Fig. 5 provides a specific example of OHC characteristics that would be sufficient to implement the proposed cochlear amplifier in the context of the cochlear model presented here.

IV. CONCLUSIONS

The cochlear model presented in this paper suggests that OHCs are primarily responsible for the sharp tuning observed in cochlear mechanics. The OHC is modeled by explicit transducer characteristics which have only low-pass tuning in isolation, but acquire bandpass tuning when placed in the cochlea. The enhancement of tuning is due to a mechanical feedback loop established within the cochlear partition in which contraction of the OHC directly influences displacement of the OHC hair bundles. At low frequencies, OHC contraction is in-phase with BM displacement toward scala vestibuli and, therefore, suppresses the shearing between TM and RL. As the frequency approaches CF, OHC contraction lags behind BM displacement. When OHC contraction becomes in-phase with BM displacement toward scala tympani, it adds to the shearing between TM and RL. In this way, OHC motility amplifies the vibration of the BM and, at the same time, sharpens the tuning of the mechanical vibrations delivered to the inner hair cells.

ACKNOWLEDGMENTS

This work was supported by a research grant from NIH-NIDCD. E. de Boer and two anonymous reviewers provided many helpful comments.

Allen, J. B. (1980). "Cochlear micromechanics—A physical model of transduction," J. Acoust. Soc. Am. 68, 1660–1679.

Allen, J. B. (1983). "Magnitude and phase frequency response to single tones in the auditory nerve," J. Acoust. Soc. Am. 73, 2071–2092.

Ashmore, J. F. (1987). "A fast, motile response in guinea-pig outer hair cells: The cellular basis of the cochlear amplifier," J. Physiol. 388, 323–347.

Brownell, W. E., Bader, C. E., Bertrand, D., and deRibaupierre, Y. (1985). "Evoked mechanical responses of isolated outer hair cells," Science 227, 194–196.

Brundin, L., Flock, A., and Canlon, B. (1989). "Sound-induced motility of isolated outer hair cells is frequency specific," Nature 34, 814–816.
Cody, A. R., and Russell, I. J. (1987). "The responses of hair cells in the basal turn of the cochlea to tones," J. Physiol. 383, 551–569.
Dallos, P. (1986). "Neurobiology of the cochlear inner and outer hair cells," Hear. Res. 22, 185–198.
Denk, W., and Webb, W. W. (1989). "Simultaneous recording of fluctuations of hair-bundle deflection and intracellular voltage in saccular hair cells," in *Cochlear Mechanisms*, edited by J. P. Wilson and D. T. Kemp (Academic, London), pp. 125–134.
Evans, B., Hallworth, R., and Dallos, P. (1991). "Outer hair cell electromotility: The sensitivity and vulnerability of the DC component," Hear. Res. 52, 288–304.
Geisler, C. D. (1986). "A model of the effect of outer hair cells on cochlear vibration," Hear. Res. 24, 125–131.
Geisler, C. D., and Shan, X. (1991). "A model for cochlear vibrations based on feedback from motile outer hair cells," in *Mechanics and Biophysics of Hearing*, edited by P. Dallos, C. D. Geisler, J. W. Matthews, M. A. Ruggero, and C. R. Steele (Springer-Verlag, New York), pp. 86–95.
Geisler, C. D. (1991). "A model using feedback from motile outer hair cells," Hear. Res. 54, 105–107.
Gold, T. (1948). "Hearing II. The physical basis of action in the cochlea," Proc. R. Soc. London Ser. B 135, 492–498.
Jones, K. L., and Kim, D. O. (1988). "A three-degree-of-freedom active micromechanical model of the cochlear partition," in *Cochlear Mechanisms: Structure, Function, and Models*, edited by J. P. Wilson and D. T. Kemp (Plenum, London), pp. 83–92.
Kim, D. O., Siegel, J. H., and Molnar, C. E. (1979). "Cochlear nonlinear phenomenon in two-tone responses," in *Models of the Auditory System and Related Signal Processing Techniques*," Scand. Audiol. Suppl. 9, 63–81.
Kim, D. O., Neely, S. T., Molnar, C. E., and Matthews, J. W. (1980). "An active cochlear model with negative damping in the cochlear partition: Comparison with Rhode's ante- and postmortem results," in *Psychological, Physiological and Behavioral Studies in Hearing*, edited by G. van den Brink and F. A. Bilsen (Delft U. P., Delft, The Netherlands), pp. 7–14.
Kolston, P. J., de Boer, E., Viergever, M. A., and Smoorenburg, G. F. (1990). "What type of force does the cochlear amplifier produce?," J. Acoust. Soc. Am. 88, 1794–1801.
Liberman, M. C. (1978). "Auditory nerve response from cats raised in a low-noise chamber," J. Acoust. Soc. Am. 63, 442–455.
Liberman, M. C., and Dodds, L. W. (1984). "Single-neuron labeling and chronic cochlear pathology. III. Stereocilia damage and alteration to threshold tuning curves," Hear. Res. 16, 55–74.
Lynch, T. J., Nedzelnitsky, V., and Peake, W. T., (1981). "Input impedance of the cochlea of the cat," J. Acoust. Soc. Am. 68, 1676–1689.
Matthews, J. W. (1980). "Mechanical modeling of the nonlinear phenomena observed in the peripheral auditory system," doctoral thesis, Washington Univ., St. Louis, MO.
Mountain, D. C., Hubbard, A. E., and McMullen, T. A. (1988). "Electromechanical processes in the cochlea," in *Mechanics of Hearing*, edited by E. de Boer and M. A. Viergever (Delft U. P., The Netherlands), pp. 119–126.
Nedzelnitsky, V. (1980). "Sound pressures in the basal turn of the cat cochlea," J. Acoust. Soc. Am. 68, 1676–1689.
Neely, S. T., and Kim, D. O. (1983). "An active cochlear model showing sharp tuning and high sensitivity," Hear. Res. 9, 123–130.
Neely, S. T., and Kim, D. O. (1986). "A model for active elements in cochlear biomechanics," J. Acoust. Soc. Am. 79, 1472–1480.
Santos-Sacchi, J. (1989). "Asymmetry in voltage dependent movements of isolated outer hair cells from the organ of Corti," J. Neurosci. 9, 2964–2967.
Santos-Sacchi, J. (1991). "Fast outer hair cell motility: how fast is fast?," in *Mechanics and Biophysics of Hearing*, edited by P. Dallos, C. D. Geisler, J. W. Matthews, M. A. Ruggero, and C. R. Steele (Springer-Verlag, New York), pp. 69–75.
Sellick, P. M., Patuzzi, R., and Johnstone, B. M. (1982). "Measurement of basilar membrane motion in the guinea pig using the Mossbauer technique," J. Acoust. Soc. Am. 65, 1007–1018.
Viergever, M. A. (1978). "On the physical background of the point impedance characterization of the basilar membrane in cochlear mechanics," Acustica 39, 292–297.
Viergever, M. A., and Diependaal, R. J. (1986). "Quantitative validation of models using the Liouville-Green approximation," Hear. Res. 21, 1–15.